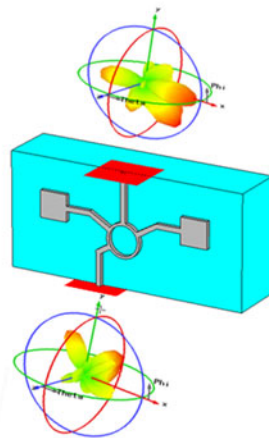# Optimization of a Novel Nano Antenna With Two Radiation Modes Using Kriging Surrogate Models

Abdel-Karim S.O. Hassan
Ahmed S. Etman
Ezzeldin A. Soliman, *Senior Member, IEEE*

A novel nano antenna with two radiation modes

Optimization of a Novel Nano Antenna With Two Radiation Modes Using Kriging Surrogate Models

Abdel-Karim S.O. Hassan,[1] **Ahmed S. Etman** (ID),[1]
and Ezzeldin A. Soliman,[2] *Senior Member, IEEE*

[1]Department of Engineering Mathematics and Physics, Faculty of Engineering, Cairo University, Giza 12613, Egypt
[2]Department of Physics, School of Sciences and Engineering, The American University in Cairo, New Cairo 11835, Egypt

Abstract: In this paper, a novel nano antenna with two radiation modes is introduced. The structure of this nano antenna consists of a ring coupler and two patch antennas placed on a SiO_2 substrate. The direction of the main lobe of the radiation pattern of this nano antenna can be adjusted to be either in the broadside or the endfire direction. The proposed nano antenna is optimized to minimize the losses and to maximize the radiation efficiency in addition to achieve maximum discrimination between the two desired directions of the main beam. In optimizing the proposed structure, the computationally expensive full-wave electromagnetic simulation is replaced by cheaper surrogate models, which are kriging models. Two optimization techniques, namely multi-objective particle swarm with preference ranking organization METHod for enrichment evaluations method and design centering using the normed distances, are used to obtain the optimal values of the design parameters. A convergence test is performed to ensure the validity of the obtained simulation results. A sensitivity analysis is performed to show how the manufacturing tolerance in each design parameter is affecting the performance of the proposed nano antenna.

Index Terms: Plasmonics, nano antennas, two radiation modes, kriging models, design centering, multi-objective particle swarm.

1. Introduction

The concept of the reconfigurable/adjustable antenna is to use a single antenna to perform differently from the points of view of the operating frequency, polarization, or radiation pattern. Reconfigurable antennas are suitable for many applications especially when several operating modes are required from a single antenna. These applications include Multiple Input Multiple Output (MIMO) communication systems [1]–[9], cellular and personal communication systems [10]–[13], interference rejection [14], [15], wireless network security [16], and military applications [17]. A reconfigurable nano antenna is a reconfigurable antenna which operates in the optical range of frequency. Consequently, its dimensions should be scaled down to the nanometer scale.

Nano antenna can efficiently convert free propagating optical electromagnetic wave into localized or guided wave and vice versa. Nowadays, there exist several publications in reconfigurable nano antennas. For example, a frequency reconfigurable nano antenna is designed in [18] by changing

the bias on the graphene. A reconfigurable multiple-input multiple-output graphene based antenna is proposed in [6]. A frequency reconfigurable antenna based on graphene stack is introduced in [19]. In [20], a multi-resonance operation is achieved from a log-periodic toothed nano antenna based on graphene. In [21], a nano antenna that is capable of reversing the radiation direction at the same resonance frequency is designed. In [22], a beam reconfigurable antenna operating in the THz band is proposed. This antenna consists of two layer of graphene and its radiation direction can be controlled through changing the bias voltage applied on each layer. In [23], a leaky-wave antenna is used to construct a reconfigurable antenna that allows both frequency tuning and beam steering in the terahertz band. In [24], a dual-polarized nano antenna that can manipulate the two orthogonal polarizations is introduced.

A novel design of reconfigurable nano antenna along with its optimization are introduced in this work. This nano antenna has the ability to switch its radiation lobe direction to alternate between two perpendicular directions, the broadside and the endfire direction. The former direction is perpendicular to the plane of the antenna, while the latter is tangential to the antenna's plane. The operating frequency of the antenna is 193 THz, which is commonly used by optical communication systems. In this frequency regime, the metals don't behave as perfect conductors, and allow electromagnetic field to penetrate them to some extent, which leads to losses. The optimization of the antenna aims to minimize these losses, minimize the deviation of the main lobe from the ideal broadside and endfire directions, and to maximize the radiation efficiency. The design is performed in three steps: a ring coupler is designed, then a rectangular patch is prepared, and finally two such patches are connected to the ring coupler to finalize the proposed radiating system. The optimization is performed on each design step. Entire-based optimization is performed on the overall antenna and its results are compared with the component-based optimization results.

The optimization of the proposed nano antenna requires multitude function evaluations. Each evaluation is performed by running a computationally expensive full-wave electromagnetic simulation using CST Microwave Studio [25]. This renders the optimization process very slow and consequently it may be prohibitive. To overcome this problem, the direct optimization of the exact high-fidelity model of the antenna is replaced by iterative updating and re-optimization of a cheaper surrogate model. Surrogate model may be a physical or mathematical model. The physical models are constructed based on particular knowledge about the physical system. They are more expensive to evaluate than the mathematical models. Furthermore, physical models are usually dedicated and so they can't be reused in other systems. On the other hand, mathematical models can be constructed without any knowledge of the physical system, which makes them generic. Such models based on algebraic models, are often very cheap in evaluation but they require considerable amount of data to ensure reasonable accuracy.

In this paper, a mathematical model called the kriging model which is developed by Krige [26] is used to build surrogate models [27], [28] of the responses of the nano antenna. Kriging is an interpolation method that predicates unknown output values at unsampled locations. After constructing the cheap surrogate models for the antenna responses, optimal values of the design parameters are obtained by applying optimization techniques on the surrogate models. In this work, two different optimization approaches are used in finding the optimal design. The first is a multi-objective optimization algorithm which handles simultaneous optimization of two or more conflicting objective functions. In Multi-Objective Optimization Problems (MOPs), there is no single solution that is always the best when measured on all objectives but rather there exist a set of alternative solutions. This set of solutions forms the pareto optimal set [29]. The points in the pareto optimal set are characterized by the fact that their cost cannot be improved in one objective without being worsened from the points of view of other objectives. In our work, we use Multi-Objective Particle Swarm Optimizer (MOPSO) [30], [31] to solve the multi-objective optimization problem. After obtaining the pareto optimal set, Preference Ranking Organization METHod for Enrichment Evaluations (PROMETHEE) [32] is applied to obtain a single point. The second optimization approach used in finding the optimal design is a design centering approach. Design centering is a process that attempts to find the best nominal values of the system design parameters which make the design more robust against the system fluctuations [33]. In implementing this approach, the original
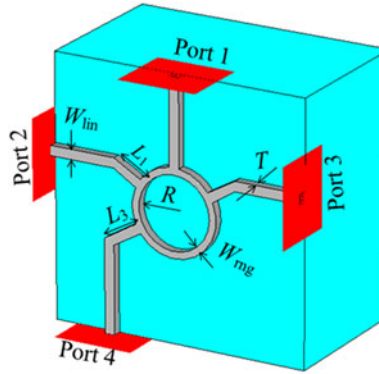
Fig. 1. Structure of the ring coupler.

multi-objective optimization problem is reformulated by specifying bounds on the design objective functions and so the optimization problem is transformed to find a design point that satisfies a set of constraints (design specifications). There exist a multitude of design points that satisfy these design specifications, however design centering seeks for the nominal design parameter values that maximize the probability of satisfying the design specifications (yield function). Hence in this paper, the aim of using the design centering in the optimization of the proposed nano antenna is to obtain a design point which is immune against the statistical fluctuations of the design parameters with the possibility of reducing the computational effort required in comparison with the computational cost required in the multi-objective optimization algorithms. In general, there are two main approaches for solving the design centering optimization problem. The first is a statistical approach which maximizes the yield function explicitly while the second is geometrical approach in which the yield function is implicitly maximized through approximating the feasible region constructed by the design specifications by using a geometrical body whose center is taken as the design center [34]–[36]. In this work, a geometrical design centering method which is the normed distances [35], [36] is used. The results of the two optimization approaches are compared and it can be verified that the design centering approach gives more immune design against the fluctuations that may occur in the design parameters and reduces the computational effort and so it is more preferable.

Section 2 presents the proposed reconfigurable nano antenna whose performance is optimized using the optimization techniques introduced in Section 3. The optimization results are demonstrated in Section 4. The effect of varying the design parameters on the antenna performance is presented in the form of a sensitivity analysis in Section 5. The paper is concluded in Section 6.

2. Proposed Reconfigurable Nano Antenna

The proposed nano antenna is constructed by exploiting the ring coupler and the rectangular patch antenna. The ring coupler (rate-race coupler) is a 3 dB coupler [37]. It consists of a ring connected to four plasmonic strip transmission lines, as shown in Fig. 1. Each transmission line is terminated by an input/output port. The points of connection between the ring and the transmission lines are selected to be at equi-distances along one half of the ring, as shown in Fig. 1.

The scattering matrix characterizing an ideal ring coupler is

$$S = \frac{-j}{\sqrt{2}} \begin{bmatrix} 0 & 1 & 1 & 0 \\ 1 & 0 & 0 & 1 \\ 1 & 0 & 0 & -1 \\ 0 & 1 & -1 & 0 \end{bmatrix}. \tag{1}$$
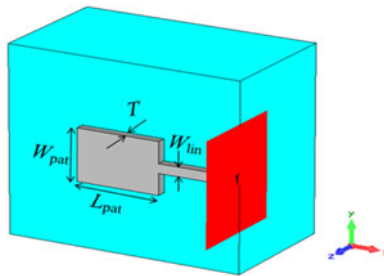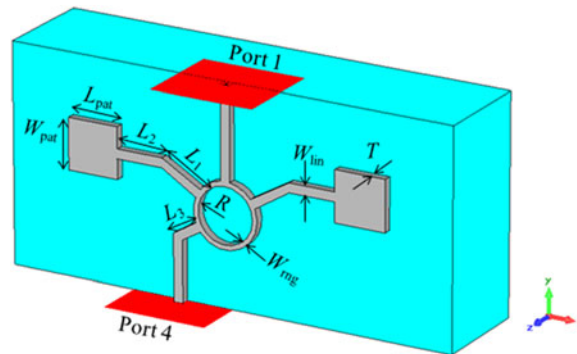
Fig. 2. Structure of the patch antenna.

Fig. 3. Structure of the proposed reconfigurable nano antenna.

The function of the ring coupler is that when an input signal is applied on port 1, it will be evenly distributed between port 2, port 3 with the same phase, while port 4 will be isolated. Conversely, when the input signal is applied on port 4, it will be split evenly between port 2, and port 3 but with 180° phase difference, while port 1 will be isolated. These ways of power distribution occur when the electric circumference of the ring is one and half guided wavelength and the characteristic impedance of the transmission line forming the rings is 1.414 times that of the feeding transmission lines.

The patch antenna [38] is a simple antenna that can be easily fed and fabricated. If the electric length of the patch equals half of a guided wavelength, the fringing electric fields at the edges of the patch are maximum and in the same direction, which gives rise to radiation. The direction of maximum radiated power is the broadside direction, which is perpendicular to the patch. The structure of the rectangular patch antenna fed with a plasmonic strip transmission line is shown in Fig. 2.

The proposed reconfigurable nano antenna is formed by integrating two rectangular patches with the ring coupler, as shown in Fig. 3. The two patches are replacing the termination input/output ports 2 and 3 of the ring coupler. Silver is selected for fabricating the ring, patches and transmission lines. It is modeled using Drude model permittivity function with $\varepsilon_\infty = 3.7$, plasma oscillation frequency of $\omega_p = 1.39{*}10^{16}$ rad/s, and a plasma collision frequency of $\gamma = 3.2258{*}10^{13}$ 1/s. The nano antenna is located on top of an infinite SiO$_2$ substrate with refractive index of 2.1. A sufficient space is inserted between the nano antenna and the Perfect Matched Layer (PML) boundary box used in simulation. CST Microwave Studio is used for that purpose. Numerical convergence test is always performed to ensure that further mesh refining doesn't affect the results significantly. The proposed nano antenna has nine geometrical parameters: the length and width of the patch (L_{pat}, W_{pat}), the radius of the ring (R), the length of the lines connecting the patches to the ring (L_1 and L_2). The length of the line segment connecting the ring to the feeding line of port 4 (L_3), the width of the ring (W_{rng}), the width of the lines (W_{lin}), the thickness of the metal layer forming the proposed reconfigurable antenna (T), as demonstrated in Fig. 3.
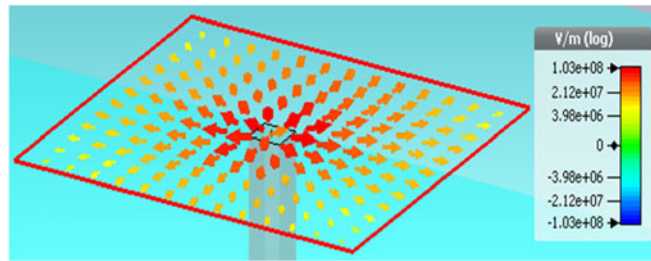
Fig. 4. Modal electric field distribution of the plasmonic transimission line at 193 THz.
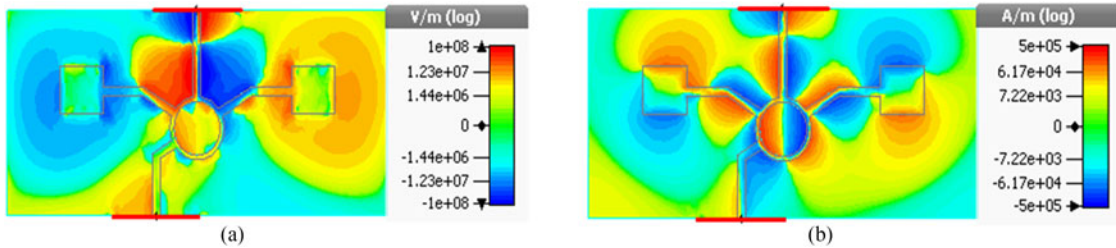

Fig. 5. Field distribution at 193 THz resonance frequency due to excitation from port 1: (a) Ex component, and (b) Hz component.
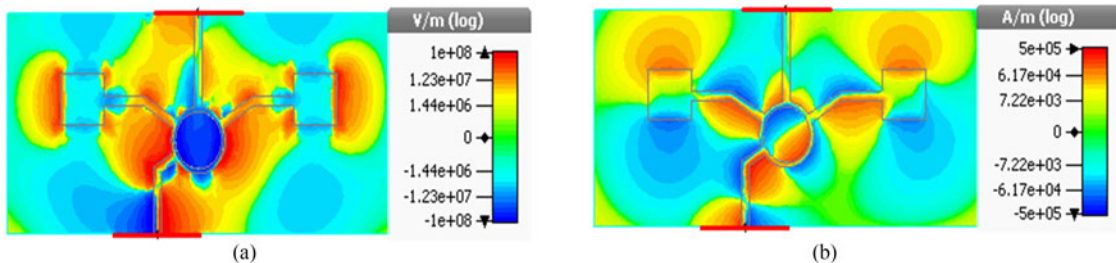

Fig. 6. Field distribution at 193 THz resonance frequency due to excitation from port 4: (a) Ex component, and (b) Hz component.

The selected operating frequency of the proposed nano antenna is 193 THz (1550 nm wavelength), which is commonly used by optical communication systems. The nano antenna is simulated using the CST frequency domain solver, which is based on finite element method. An adaptive mesh is used to validate the mesh and to ensure numerical convergence.

The proposed nano antenna has two input ports (port 1 and port 4 of the ring coupler). The excited mode at the input ports is the fundamental mode only which may be generated from electrical or laser input. Modal electric field distribution of the plasmonic transimission line at 193 THz is shown in Fig. 4. When the excitation is made from port 1, the x- and z-components of the electric and magnetic field, respectively, of the two patches will be out of phase as shown in Fig. 5(a) and (b), respectively. This leads to destructive radiation interference along broadside direction, while constructive interference can be achieved along the endfire direction. On the other hand, when exciting from port 4, the x-/z-component of the electric/magnetic field of the two patches will be in phase as shown in Fig. 6(a) and (b). Consequently, constructive interference is ensured along the broadside direction, while destructive interference can be adjusted to occur along the endfire direction. The values of the design parameters used in the field simulation are those obtained from the component-based optimization by using the normed distances that will be shown in

Section 4.1.3. However using the other optimal points (presented in Sections 4.1.3 and 4.2) will give almost the same field distributions. Each of the two radiation modes could be obtained by exciting from the appropriate port (port 1 for the endfire and port 4 for the broadside). Alternating between the two radiation modes based on the excited port is guaranteed by the optimization process.

As the metals don't behave as perfect conductors in optical frequency regime, they allow electromagnetic field penetration to some extent. This results in considerable amount of power dissipation. In addition to this dissipation kind of loss, there exists reflection loss at the excitation port as well as transmission loss to the other unexcited port. These power losses need to be minimized. The power dissipation can be minimized by maximizing the radiation efficiency. The reflection and transmission losses can be minimized by minimizing the magnitude of the S-parameters ($|S_{11}|$, $|S_{41}|$, $|S_{14}|$, $|S_{44}|$). For good control of the radiation beam direction, angles θ_1, θ_2 are defined and have to be minimized. The first angle, θ_1, measures the angular difference between the main beam and the endfire direction if the excitation is made from port 1. On the other hand, the difference between the main beam and the broadside direction due excitation from port 4 is measured using θ_2.

Two design approaches are performed to optimize the proposed antenna. In the first one, the optimization of the proposed antenna is performed through three steps as follows: optimizing the ring coupler followed by the patch antenna then the integration of components. The optimal parameter values obtained in each step of this approach are used as initial values for the next step. In the second approach, the optimization process is made directly in one step on the entire nano antenna structure.

The steps of the first approach are the following. First, the geometrical dimensions of the ring coupler shown in Fig. 1 are optimized to achieve minimum dissipation, reflection, and transmission loss and to distribute the remaining power evenly between the output ports, which will be terminated by the radiating patches in the following step. In other words, it is required to minimize the magnitude of each of (S_{11}, S_{41}, S_{14}, S_{44}) and to make the magnitude of each of (S_{21}, S_{31}, S_{24}, S_{34}) as close as possible to -3 dB. It is also required to keep the phase difference between S_{24} and S_{34} as close as possible to 180º. Second, the geometrical parameters of single patch antenna, shown in Fig. 2, are optimized to minimize the reflection loss, the deviation between the broadside and the main beam direction, and to maximize the radiation efficiency. In doing this optimization, the initial values of width and thickness of the feeding line connected to the patch, (W_{lin}, T), are the same as that of optimum values of the same variables obtained in the previous step. Finally the geometrical dimensions of the integrated reconfigurable antenna are optimized to minimize the reflection and transmission loss, the deviation between the main beam direction and (the endfire, the broadside) when exciting from (port 1 or port 4) and to maximize radiation efficiencies when exciting from both input ports.

3. Optimization Approaches

As the simulation time required to perform a single simulation run of the proposed antennna is very long, the direct optimization may be prohibitive and so the simulation runs have to be accelerated. This idea has been used in many publications as [34], [36], [39]. To perform the optimization process of the proposed nano antenna, surrogate models of its responses are constructed. Here we use kriging models [28] and then we use two different optimization approaches to solve the optimization problem. The first approach is the multi-objective particle swarm optimization [30], [31] which is a metaheuristic method used to solve multi-objective optimization problems. To obtain a single point to use in design, PROMETHEE [32] is applied on the optimal pareto set obtained from MOPSO [31]. And the second is the normed distances [35], [36] which is a geometrical design centering technique.

3.1 Kriging Models

A kriging model is a combination of a polynomial model plus localized departures of the form:

$$y(\mathbf{x}) = h(\mathbf{x}) + z(\mathbf{x}) \tag{2}$$

where $y(\mathbf{x})$ is the unknown required function, $h(\boldsymbol{x})$ is an approximation (polynomial) function and it can be represented as a linear combination of some regression functions. In this work, quadratic polynomials are used. $z(\boldsymbol{x})$ is the realization of a stochastic process with zero mean, variance σ^2, and non-zero covariance. The function value at any point can be estimated using linear predicator [40] as follows

$$y_{\text{est}}(\boldsymbol{x}) = \boldsymbol{h}^{\mathsf{T}}\boldsymbol{\alpha}^* + \boldsymbol{r}^{\mathsf{T}}\boldsymbol{R}^{-1}(\boldsymbol{m} - \boldsymbol{H}\boldsymbol{\alpha}^*) \tag{3}$$

where $\boldsymbol{h}$ is a $N \times 1$ vector containing the values of the regression functions evaluated at $\boldsymbol{x}$, $\boldsymbol{R}$ is $N_s \times N_s$ matrix whose elements represent the correlation between $\boldsymbol{z}$ values at the sample points, where N_s is the number of the sample points. $\boldsymbol{r}$ is $N_s \times 1$ vector containing the correlation between $\boldsymbol{z}$ values at $\boldsymbol{x}$ and at the sample points. $\boldsymbol{H}$ is $N_s \times N$ matrix, whose elements represent the values of the regression functions at the sample points $\boldsymbol{m}$ is a $N_s \times 1$ vector whose each component represents the value of y evaluated at the corresponding sample point. The value of $\boldsymbol{\alpha}^*$ is given by:

$$\boldsymbol{\alpha}^* = \left(\boldsymbol{H}^{\mathsf{T}}\boldsymbol{R}^{-1}\boldsymbol{H}\right)^{-1}\boldsymbol{H}^{\mathsf{T}}\boldsymbol{R}^{-1}\boldsymbol{m} \tag{4}$$

3.2 Multi-Objective Particle Swarm Optimization

Multi-objective optimization problem is a problem which has more than one objective function that we need to optimize simultaneously. These objectives are normally conflicting which means that there is no single solution that is the best for all objectives in these problems. Instead, there exist good trade-off solutions that represent the best possible compromises among the objectives. These solutions form a set called pareto optimal set (P*). Each design point in this set is non-dominated which means that there is no other point in the design space (DS) that is better than it in all objectives.

$$P^* = \left\{\boldsymbol{x} \in \text{DS} \mid \neg \exists \boldsymbol{z} \in \text{DS} \wedge \boldsymbol{F}(\boldsymbol{z}) \prec \boldsymbol{F}(\boldsymbol{x})\right\} \tag{5}$$

where $\boldsymbol{F}(\boldsymbol{x})$ is the vector of the objective functions evaluated at $\boldsymbol{x}$. $\boldsymbol{F}(\boldsymbol{z}) \prec \boldsymbol{F}(\boldsymbol{x})$ means that each component in $\boldsymbol{F}(\boldsymbol{z})$ is less than or equal its corresponding component in $\boldsymbol{F}(\boldsymbol{x})$ and there exist at least one component in $\boldsymbol{F}(\boldsymbol{z})$ which is strictly less than the corresponding component in $\boldsymbol{F}(\boldsymbol{x})$. The image of the pareto optimal set in the objective space is called the pareto front (PF*).

One of the most powerful algorithms used to obtain the pareto optimal set is the Multi-Objective Particle swarm optimization (MOPSO) [31] which is a metaheuristic algorithm based on Swarm intelligence [30]. To obtain a single design from the pareto optimal set obtained from MOPSO, we use PROMETHEE [32].

3.3 Design Centering Using Normed Distances

Design centering using normed distances [35], [36] is a geometrical approach for obtaining the design center point of a feasible region (FR) which is a region in the parameter space that can be identified by specifying either upper or lower bounds on the system performance properties.

The design parameters are in general random variables distributed with joint probability density function (pdf) $\varnothing(\boldsymbol{x}, \boldsymbol{\psi})$ where $\boldsymbol{\psi}$ is the vector of different distribution parameters. Accordingly, the yield (probability of satisfying the design specifications) is defined as

$$Y(\boldsymbol{\psi}) = \text{Prob}(\boldsymbol{x} \in \text{FR}) = \int_{\text{FR}} \phi(\boldsymbol{x}, \boldsymbol{\psi})d\boldsymbol{x}. \tag{6}$$

Assuming that, the probability density function is dependent only on the nominal parameter vector x^0. The design centering problem can be formulated as

$$\max_{x^0} \left(Y(x^0) = \int_{FR} \phi(x, x^0) dx \right). \tag{7}$$

Practically the system parameters are assumed to be normally distributed with pdf given by

$$\phi(x, x^0) = \frac{1}{(2\pi)^{n/2} \sqrt{|C|}} e^{-\frac{1}{2}(x-x^0)^T C^{-1}(x-x^0)} \tag{8}$$

where C is the covariance matrix. The normed distance between x^0 and the hypersurface $f(x) = 0$ is given by

$$\beta = \min_x \sqrt{(x - x^0)^T C^{-1} (x - x^0)}$$

$$\text{such that } f(x) = 0. \tag{9}$$

The design centering problem can be solved as follows [41]:

$$\max_{x^0} \left(\min_{i=1,2,\dots l} \beta_i \right). \tag{10}$$

where $\beta_i, i = 1, 2, \dots, l$ is the normed distance from x^0 to the constraint boundary $f_i(x) = 0$.

3.4 Optimization Algorithm

An algorithm for the optimization approaches can be summarized in the following steps:
1. Generate sample points using Latin hypercube sampling.
2. Evaluate the function values using the high fidelity model (using CST simulation).
3. Construct kriging surrogate models using the function values obtained at step 2.
4. Find an optimal design using MOPSO or normed distances.
5. If we reach optimum point then we terminate, else generate another sample points and perform step 2 then add these points to the pervious sample points then go to step 3.

4. Optimization Results

The optimization techniques discussed in Section 3 are going to be applied on the novel reconfigurable nano antenna introduced in Section 2 using the two different design approaches previously outlined.

4.1 Component-Based Optimization

In this subsection, the optimization is carried out in three steps. The results of each step are presented and discussed.

4.1.1 Ring Coupler Optimization

In this step, the optimization process is applied on the ring coupler shown in Fig. 1. The design parameters are $[R, L_1, L_3, W_{lin}, T, W_{rng}]$. The optimization goals can be written as follows

$$\min |S_{11}|, |S_{41}|, |S_{14}|, |S_{44}|$$

$$\max |S_{21}|, |S_{31}|, |S_{24}|, |S_{34}| \tag{11}$$

$$\min | |\angle S_{24} - \angle S_{34}| - 180°|.$$

TABLE I
Results of the Ring Coupler Optimization

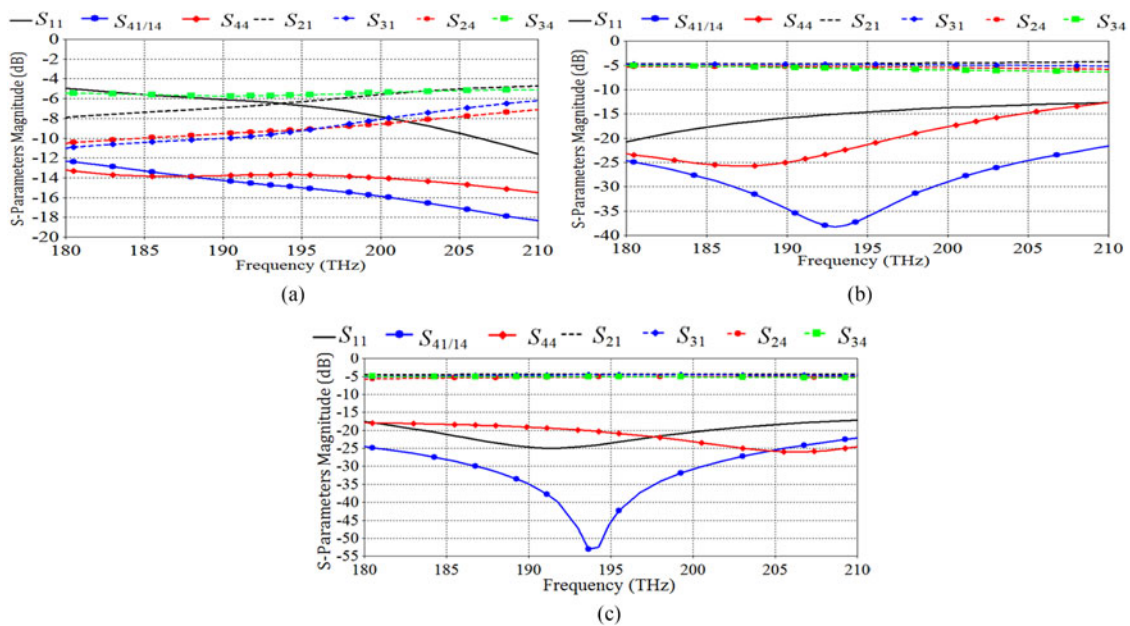|	Initial	MOPSO Final	Normed Distances Final		Initial	MOPSO Final	Normed Distances Final
R (nm)	160	188.252	199.617	$|S_{14}|$ (dB)	-14.66	-38.24	-46.05
L_1 (nm)	100	96.241	148.656	$|S_{44}|$ (dB)	-13.65	-24.09	-19.82
L_3 (nm)	350	160.31	204.634	$|S_{21}|$ (dB)	-6.54	-4.63	-4.35
W_{lin}(nm)	40	28.3754	40.839	$|S_{31}|$ (dB)	-9.67	-4.74	-4.76
T (nm)	45	36.192	44.358	$|S_{24}|$ (dB)	-9.33	-5.22	-5.13
W_{rng} (nm)	35	24.561	23.5419	$|S_{34}|$ (dB)	-5.7	-5.54	-5.07
$|S_{11}|$ (dB)	-6.44	-14.95	-24.69	$|\angle S_{24} - \angle S_{34}|$	139.6°	187.2°	186.75°
$|S_{41}|$ (dB)	-14.66	-38.35	-46.14	Yield	0%	56%	71%
Simulation Time		26 hours	22 hours				

Fig. 7. *S*-parameters magnitude of the ring coupler versus frequency at: (a) Initial point (b) MOPSO final, and (c) Normed distances final.

This multi-objective problem is solved by using MOPSO with PROMETHEE. To solve this problem using normed distances, it is reformulated according to the following constraints

$$|S_{11}|, |S_{41}|, |S_{14}|, |S_{44}| < -10\,\text{dB}$$
$$|S_{21}|, |S_{31}|, |S_{24}|, |S_{34}| > -6\,\text{dB} \tag{12}$$
$$||\angle S_{24} - \angle S_{34}| - 180°| < 10.$$

This problem is solved using the normed distances taking parameter spread = [10, 10, 10, 2, 2, 2] nm. The results are summarized in Table I. The S-parameters at the final point of MOPSO with PROMETHEE and the normed distances are comparable. However the normed distances method gives a better yield value and a lower simulation time. So the design obtained using the normed distances is more immune against the system's fluctuations with reduced computational cost The S-parameters magnitudes versus frequency are shown in Fig. 7. The phase of S_{24}, S_{34} are shown in Fig. 8. The potential of the proposed optimization techniques is evident, as it succeeded
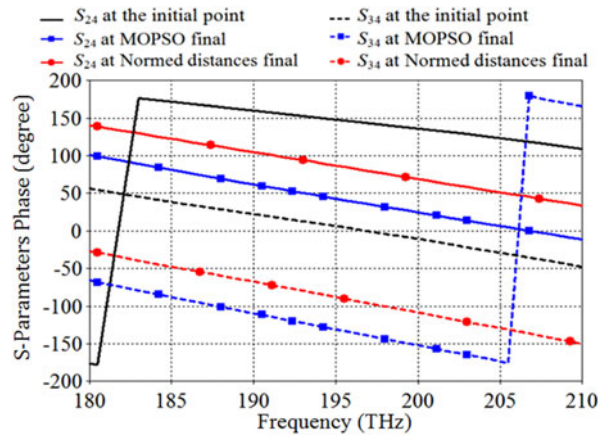
Fig. 8. Phase of S_{24}, S_{34} of the ring coupler versus frequency.

TABLE II

Results of the Patch Nano Antenna Optimization

	MOPSO		Normed distances	
	Initial	Final	Initial	Final
W_{pat} (nm)	300	307.4	300	301.7
L_{pat} (nm)	300	403.4	300	422.9
W_{lin} (nm)	28.38	49.6	40.839	54.66
T (nm)	36.19	51.6	44.358	44.99
$|S_{11}|$ (dB)	-3.69	-10.9	-4.44	-12.9
θ_1	27°	1°	21°	2°
η_{rad}	0.855	0.95	0.92	0.95
Yield	0%	87%	0%	95%
Simulation Time	18 hours		14 hours	

in bringing the insertion losses close to -4 dB, while the transmission losses are less than -15 dB. Moreover, the phase difference between S$_{24}$ and S$_{34}$ is adjusted to be very close to 180º as required.

4.1.2 Patch Nano Antenna Optimization

In this step, the patch nano antenna dimensions [W$_{pat}$, L$_{pat}$, W$_{lin}$, T] are optimized for these objectives:

$$\min |S_{11}|, \theta_1$$

$$\max \eta_{rad}. \tag{13}$$

where S$_{11}$ is the reflection coefficient, η_{rad} is the radiation efficiency, θ_1 is the angle between the main lobe direction and the broadside direction. This optimization problem is solved using MOPSO with PROMETHEE. Then, the optimization problem is reformulated to be solved using normed distances by imposing the following constraints

$$|S_{11}| < -10\,\text{dB}$$

$$\theta_1 < 10$$

$$\eta_{rad} > 0.8. \tag{14}$$

The values of W$_{lin}$, T in the initial point are taken form the final point in step 1. The parameter spread used in the normed distances and the yield evaluation is [10, 10, 2, 2] nm. Table II lists the simulation results of Step 2. The objective functions values at the final point of MOPSO with
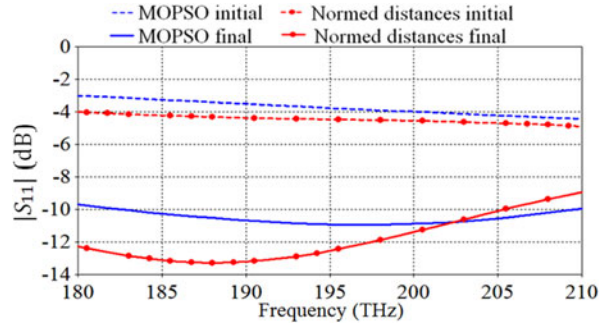
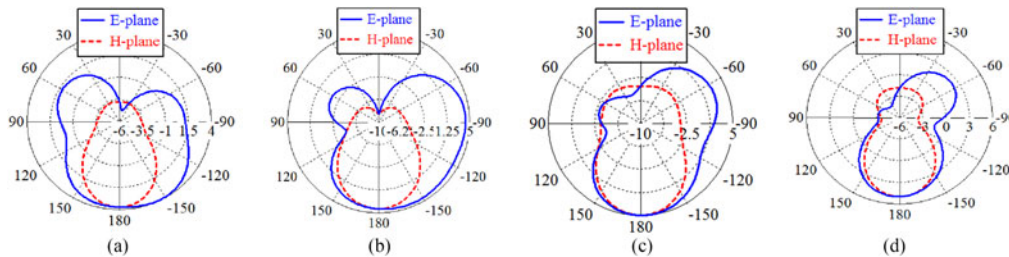Fig. 9. $|S_{11}|$ of the patch nano antenna versus frequency.

Fig. 10. Radiation pattern of the patch nano antenna at (a) the initial point of MOPSO (b) the initial point of Normed distances (c) the final point of MOPSO (d) the final point of Normed distances.

PROMETHEE and the normed distances are comparable however the normed distances method is better in terms of the yield value and the simulation time. The magnitudes of the reflection loss, S_{11}, versus frequency are shown in Fig. 9. The optimization process leads to a significant reduction in the reflection loss as required. The corresponding initial radiation patterns in the E-plane (xz-plane), which is the plane of asymmetry, and in the H-plane (yz-plane) are presented in Fig. 10(a) and (b). The final radiation pattern after optimization is plotted in Fig. 10(c) and (d). It is obvious that the final radiation patterns of the optimized nano antenna using both optimization techniques are way better than the initial ones with maximum radiation power density along the broadside direction and the beam is narrower as required. In all radiation pattern plots, it is clear that the back-side radiation is stronger than the front-side. This can be attributed to the low value of the wave impedance of the dielectric half-space if compared to that of the free-space at the top-side.

4.1.3 Optimization of the Integration of Components

In this step, optimization techniques are applied on the integrated components forming the proposed reconfigurable nano antenna. The initial values of the design parameters of this step are those final values of the previous optimization steps. The design parameters are $[W_{pat}, L_{pat}, R, L_1, L_2, L_3, W_{lin}, T, W_{rng}]$. The parameter spread adopted in the normed distances and the yield evaluation is [10, 10, 10, 10, 10, 10, 2, 2, 2] nm. The optimization goals in this final step are

$$\min |S_{11}|, |S_{41}|, |S_{14}|, |S_{44}|, \theta_1, \theta_2$$

$$\max \eta_{rad1}, \eta_{rad4}. \tag{15}$$

where η_{rad1}, η_{rad4} are the radiation efficiencies when exciting from port 1 and port 4, respectively. θ_1 is the angular difference between the endfire and the main beam when exciting from port 1. On the other hand, θ_2 measures the difference between the broadside and the main lobe direction when port 4 is excited. The problem is reformulated as design centering problem to be solved using the

TABLE III

Results of the Integration of Components Optimization

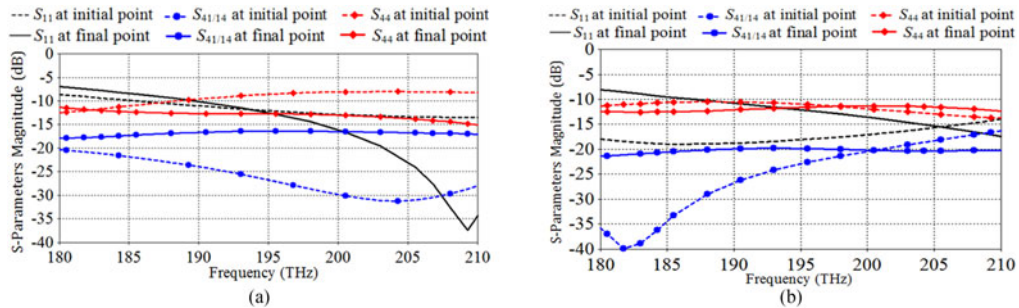|	MOPSO		Normed distances			MOPSO		Normed distances	
	Initial	Final	Initial	Final		Initial	Final	Initial	Final
W_{pat} (nm)	307.4	305.7	301.73	333.34	$|S_{11}|$ (dB)	-11.7	-11.4	-18.22	-11.6
L_{pat} (nm)	403.43	331.9	422.9	339.5	$|S_{41}|$ (dB)	-25.4	-16.4	-24.38	-19.9
R (nm)	188.25	190.39	199.6	200.65	$|S_{14}|$ (dB)	-25.4	-16.4	-24.38	-19.9
L_1 (nm)	96.241	324.1	148.7	318.9	$|S_{44}|$ (dB)	-8.94	-12.7	-10.75	-11.8
L_2 (nm)	150	383.4	150	308.4	θ_1	28°	4°	64°	0°
L_3 (nm)	160.31	100	204.6	154.6	θ_2	4°	1°	0°	1°
W_{lin} (nm)	49.552	60.85	54.66	62.73	η_{rad1}	0.883	0.898	0.889	0.913
T (nm)	51.63	55.93	44.99	57.04	η_{rad4}	0.864	0.889	0.869	0.899
W_{rng} (nm)	24.561	31.08	23.54	31.85	Yield	0%	64%	0%	81%
Simulation time	5 days		4 days and 10 hours		Overall simulation	6 days and 20 hours		5 days and 22 hours	

Fig. 11. *S*-parameters magnitudes of the reconfigurable nano antenna versus frequency at initial and final points for: (a) MOPSO and (b) Normed distances.

normed distances as follows:

$$|S_{11}|, |S_{41}|, |S_{14}|, |S_{44}| < -10\,\text{dB}$$

$$\theta_1, \theta_2 < 5$$

$$\eta_{rad1}, \eta_{rad4} > 0.8. \tag{16}$$

Table III lists the optimization results of step 3. The objective functions values at the final points are almost the same for both MOPSO with PROMETHEE and the normed distances however the normed distances method achieves better value for the yield function and reduces the simulation time. This ensures that the optimal design obtained by using the normed distances is more robust against the system's fluctuations with reduced computational cost. The corresponding *S*-parameters magnitude versus frequency are shown in Fig. 11. It is evident that the adopted optimization algorithms are capable of adjusting the *S*-parameters as required. The corresponding radiation patterns are plotted in Figs. 12 and 13. It is clear from these figures that the radiation patterns at the initial points of the two optimization techniques is way far from the desired end-fire or broadside direction if the excitation signal is applied on port 1 or port 4, respectively. The effectiveness of the proposed optimization methods can be easily noticed by comparing the initial radiation patterns plotted in Fig. 12 to the final ones presented in Fig. 13. The radiation main lobe is very well adjusted along the end-fire direction if port 1 is excited, and along the broadside direction if port 4 is excited as shown in Fig. 13(a) and (b), thanks to MOPSO. Also, normed distances technique is well capable of adjusting the radiation beams at the desired directions, as clear from Fig. 13(c) and (d).
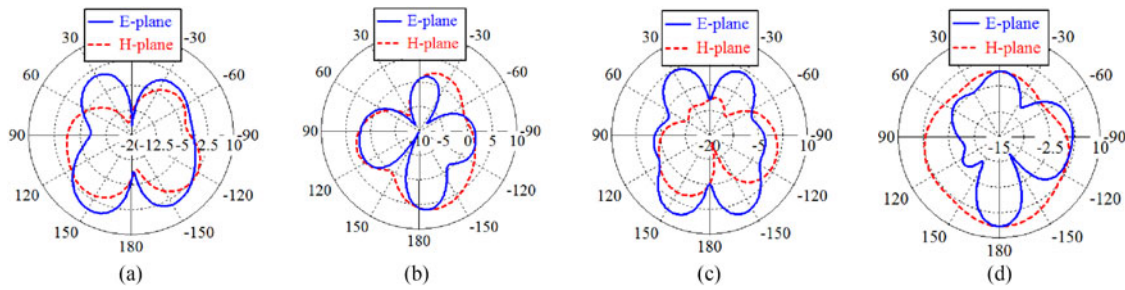
Fig. 12. Radiation pattern of the reconfigurable nano antenna at the initial point of (a) MOPSO due to excitation from port 1 (b) MOPSO due to excitation from port 4 (c) Normed distances due to excitation from port 1 (d) Normed distances due to excitation from port 4.
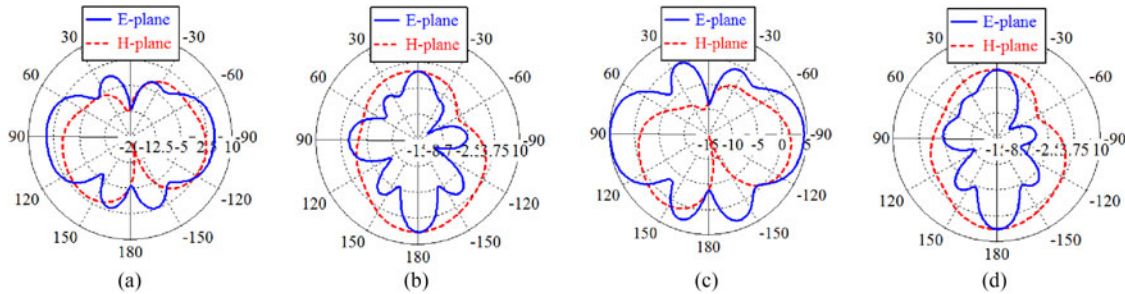

Fig. 13. Radiation pattern of the reconfigurable nano antenna at the final point of (a) MOPSO due to excitation from port 1 (b) MOPSO due to excitation from port 4 (c) Normed distances due to excitation from port 1 (d) Normed distances due to excitation from port 4.

TABLE IV

Results of the Entire-Based Optimization

| | Initial | Final | | | Initial | Final | |
		MOPSO	Normed			MOPSO	Normed
W_{pat} (nm)	300	334.263	338.952	$|S_{11}|$ (dB)	−4.17	−12.53	−11.09
L_{pat} (nm)	300	302.315	336.214	$|S_{41}|$ (dB)	−18.02	−16.05	−18.93
R(nm)	160	191.124	198.781	$|S_{14}|$ (dB)	−18.02	−16.05	−18.93
L_1 (nm)	350	321.183	314.782	$|S_{44}|$ (dB)	−8.5	−11.02	−12.38
L_2 (nm)	150	385.609	317.356	θ_1	66°	0°	0°
L_3 (nm)	100	153.34	149.315	θ_2	4°	1°	1°
W_{lin} (nm)	40	58.925	58.6145	η_{rad1}	0.798	0.883	0.901
T (nm)	45	45.8571	55.152	η_{rad4}	0.859	0.866	0.894
W_{rng} (nm)	35	41.2384	34.9125	Yield	0%	66%	79%
Simulation Time		11 days	10 days				

4.2 Entire-Based Optimization

In this approach, the optimization techniques are applied on the reconfigurable nano antenna as a whole rather on its individual components. This can be looked at as performing step 3 of the component-based optimization but without a good initial point. The parameter spread used in normed distances and in the yield evaluation is [10, 10, 10, 10, 10, 10, 2, 2, 2] nm. Table IV summarizes the optimization initial and final figures using entire-based optimization. It could be noticed that the objective functions values at the final points of MOPSO and normed distances method are comparable however the normed distances method outperforms MOPSO in terms of the yield function and the simulation time. So the deign obtained by using the normed distances
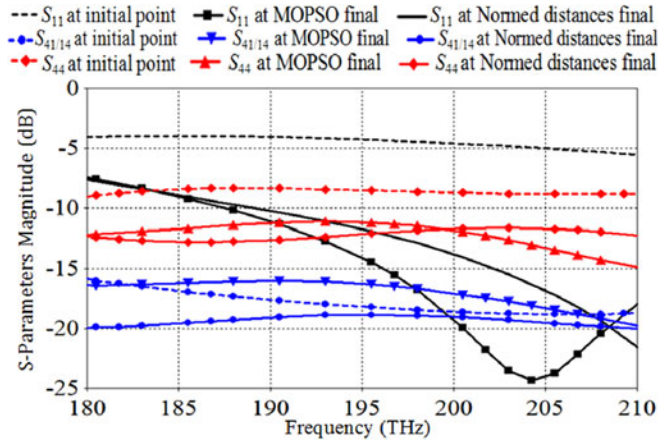
Fig. 14. *S*-parameters magnitude of the reconfigurable nano antenna versus frequency.
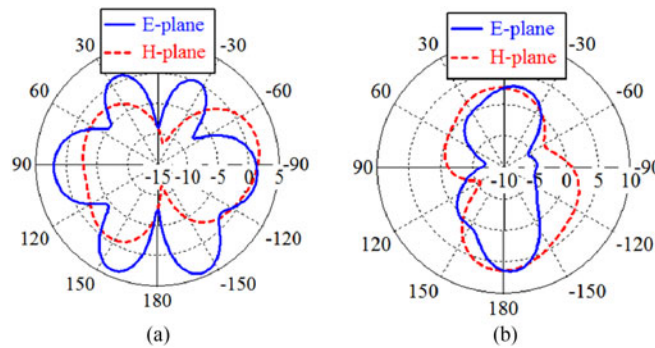

Fig. 15. Radiation pattern of the reconfigurable nano antenna at the initial point due to excitation from: (a) port 1 and (b) port 4.
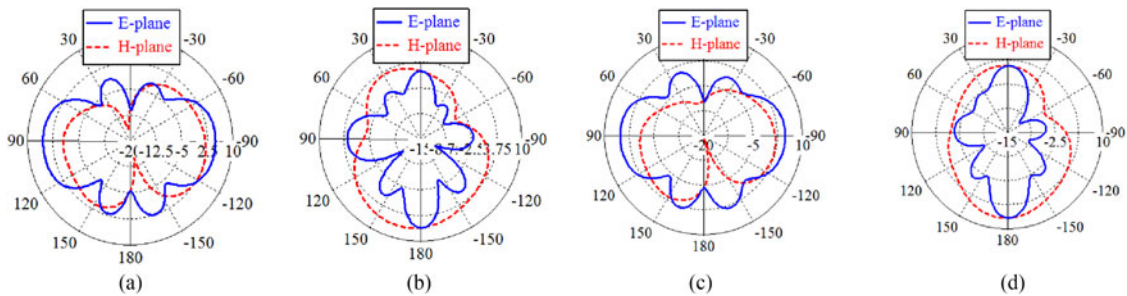

Fig. 16. Radiation pattern of the reconfigurable nano antenna at the final point of (a) MOPSO due to excitation from port 1 (b) MOPSO due to excitation from port 4 (c) Normed distances due to excitation from port 1 (d) Normed distances due to excitation from port 4.

is more immune against the system's fluctuations. Also using the normed distances reduces the computational cost. The corresponding S-parameters magnitudes versus frequency are shown in Fig. 14 and the corresponding radiation patterns are plotted in Figs. 15 and 16. Both MOPSO and normed distances optimizers are capable of adjusting the *S*-parameters and aligning the radiation beam direction to be along end-fire or broadside due to excitation from port 1 or port 4, respectively.
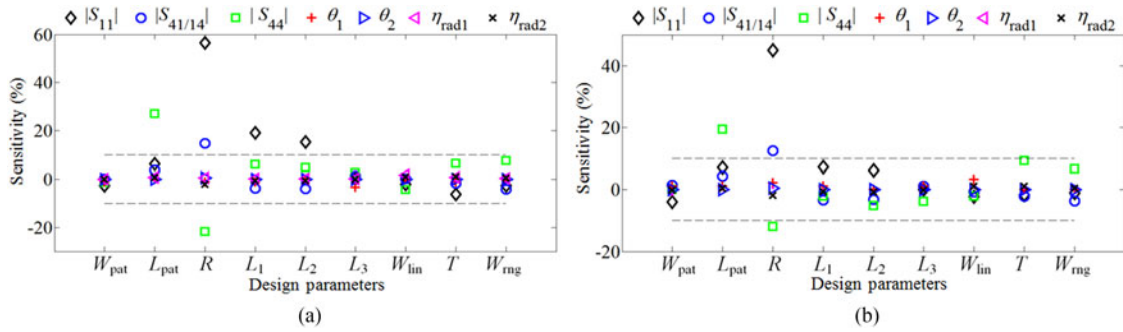
Fig. 17. Sensitivity of the objectives with respect to the design variables for the solution obtained using: (a) MOPSO and (b) Normed distances.

5. Sensitivity Analysis

As mentioned above, the proposed reconfigurable nano antenna has nine design variables and eight design objectives. This section presents a study of the impact of each design variable on the objectives. In this study, the designs obtained from component-based optimization are used. The sensitivity of each objective is calculated to identify the most effective design parameters on it. Each design variable is perturbed by 10% while the other variables remain constants. At each perturbed design, the sensitivity is calculated as follows

$$sensitivity\ of\ \ F_j = \frac{F_j(pertubed\ design) - F_j(original\ design)}{F_j(original\ design)} * 100\% \tag{17}$$

The sensitivity of the different objectives with respect to different design variables is plotted in Fig. 17 for the solutions obtained using both MOPSO and normed distances. It is clear that the design obtained from the normed distances is more immune against the variations in the design parameters as it has larger yield value compared to the design obtained from MOPSO. This can be attributed to the fact that the normed distances is a design centering technique, and hence it enhances the chance of satisfying the constraints imposed on the objectives due to reasonable variation in the design variables. It can be noticed that R is the most effective design parameters on $|S_{11}|$, $|S_{41}|$ and $|S_{14}|$. The parameters that have effect on $|S_{44}|$ are (L_{pat}, R, T). The impact on the main lobe orientation is very small while the radiation efficiency is almost unaffected when perturbing the design parameters.

6. Conclusion

A novel nano antenna design is presented for the first time in this paper. The radiation pattern of this nano antenna can be adjusted to alternate between broadside and endfire directions based on the location of the applied excitation signal. This nano antenna allows for best use of the radiated power by avoiding wasting it in unwanted directions. If the transmitter and receiver are in front of each other the antenna radiates in the broadside mode avoiding wasting power in the endfire direction. At the other hand, if the transmitter and receiver are beside each other, the antenna radiates in the endfire mode, which avoids wasting power along broadside direction. Such efficient use of power isn't provided by omni-directional conventional antennas. The selected operation frequency (wavelength) is 193 THz (1550 nm), which is commonly used by optical communication systems. The optimization of the proposed nano antenna is performed using two different approaches. The prediction of the nano antenna's responses is performed using kriging surrogate models which are much cheaper than the full-wave electromagnetic simulations counterpart. Two different optimization techniques are employed, namely MOPSO and normed distances. A sensitivity analysis is performed that shows how the manufacturing tolerance in each design parameter is affecting the performance

of the proposed reconfigurable nano antenna. Although MOPSO and normed distances achieve comparable values for the objective functions, the normed distances method achieves better value for the yield function and so the deign obtained by using the normed distances is more immune against the system's fluctuations. This is verified by the sensitivity analysis. In addition, using the normed distances results in a reduction in the computational cost. So the normed distances method is more preferable than MOPSO.

References

[1] B. A. Cetiner, H. Jafarkhani, Q. Jiang-Yuan, Y. H. Jae, A. Grau, and F. De Flaviis, "Multifunctional reconfigurable MEMS integrated antennas for adaptive MIMO systems," *IEEE Commun. Mag.*, vol. 42, no. 12, pp. 62–70, Dec. 2004.

[2] C. G. Christodoulou, Y. Tawk, S. A. Lane, and S. R. Erwin, "Reconfigurable antennas for wireless and space applications," *Proc. IEEE*, vol. 100, no. 7, pp. 2250–2261, Jul. 2012.

[3] A. Grau, J. Romeu, M. Lee, S. Blanch, L. Jofre, and F. De Flaviis, "A dual-linearly-polarized MEMS-reconfigurable antenna for narrowband MIMO communication systems," *IEEE Trans. Antennas Propag.*, vol. 58, no. 1, pp. 4–17, Jan. 2010.

[4] P.-Y. Qin, Y. J. Guo, A. R. Weily, and C.-H. Liang, "A pattern reconfigurable U-slot antenna and its applications in MIMO systems," *IEEE Trans. Antennas Propag.*, vol. AP-60, no. 2, pp. 516–528, Feb. 2012.

[5] D. Piazza, P. Mookiah, M. D'Amico, and K. R. Dandekar, "Experimental analysis of pattern and polarization reconfigurable circular patch antennas for MIMO systems," *IEEE Trans. Veh. Technol.*, vol. 59, no. 5, pp. 2352–2363, Jun. 2010.

[6] Z. Xu, X. Dong, and J. Bornemann, "Design of a reconfigurable MIMO system for THz communications based on graphene antennas," *IEEE Trans. THz Sci. Technol.*, vol. 4, no. 5, pp. 609–617, Sep. 2014.

[7] Y. Zhou, R. S. Adve, and S. V. Hum, "Design and evaluation of pattern reconfigurable antennas for MIMO applications," *IEEE Trans. Antennas Propag.*, vol. 62, no. 3, pp. 1084–1092, Mar. 2014.

[8] R. Hussain and M. S. Sharawi, "A cognitive radio reconfigurable MIMO and sensing antenna system," *IEEE Antenna Wireless Propag. Lett.*, vol. 14, pp. 257–260, 2015.

[9] H. Li, B. K. Lau, and S. He, "Design of closely packed pattern reconfigurable antenna array for MIMO terminals," *IEEE Trans. Antennas Propag.*, vol. 65, no. 9, pp. 4891–4896, Sep. 2017.

[10] Y. L. Ban, S. C. Sun, P. P. Li, J. L. W. Li, and K. Kang, "Compact eight-band frequency reconfigurable antenna for LTE/WWAN tablet computer applications," *IEEE Trans. Antennas Propag.*, vol. 62, no. 1, pp. 471–475, Jan. 2014.

[11] Y.-L. Ban, Z. X. Chen, Z. Chen, K. Kang, and J. L.-W. Li, "Reconfigurable narrow-frame antenna for heptaband WWAN/LTE smartphone applications," *IEEE Antennas Wireless Propag. Lett.*, vol. 13, pp. 1365–1368, 2014.

[12] Y. Li, Z. J. Zhang, J. F. Zheng, Z. H. Feng, and M. F. Iskander, "A compact hepta-band loop-inverted F reconfigurable antenna for mobile phone," *IEEE Trans. Antennas Propag.*, vol. 60, no. 1, pp. 389–392, Jan. 2012.

[13] Y. Li, Z. J. Zhang, J. Zheng, and Z. Feng, "Compact heptaband reconfigurable loop antenna for mobile handset," *IEEE Antennas Wirel. Propag. Lett.*, vol. 10, pp. 1162–1165, 2011.

[14] D. Rodrigo, J. Romeu, and L. Jofre, "Interference rejection using frequency and pattern reconfigurable antennas", in *Proc. Int. Symp. Antennas Propag.*, pp. 1–2, 2012.

[15] E. Nasrabadi and P. Rezaei, "A novel design of reconfigurable monopole antenna with switchable triple band-rejection for UWB applications," *Int. J. Microw. Wireless Technol.*, vol. 8, no. 8, pp. 1223–1229, Dec. 2016.

[16] P. Mookiah and K. Dandekar, "Enhancing wireless security through reconfigurable antennas," in *Proc. IEEE Radio Wireless Symp.*, 2010, pp. 593–596.

[17] A. Mehdipour, T. A. Denidni, A.-R. Sebak, C. W. Trueman, I. D. Rosca, and S. V. Hoa, "Anisotropic carbon fiber nanocomposites for mechanically reconfigurable antenna applications," in *Proc. IEEE Int. Symp. Antennas Propag.*, Orlando, FL, USA, Jul. 2013, pp. 384–385.

[18] A. Hosseinbeig, A. Pirooj, and F. B. Zarrabi, "A reconfigurable subwavelength plasmonic fano nano-antenna based on split ring resonator," *J. Magn. Magn. Mater.*, vol. 423, pp. 203–207, Feb. 2017.

[19] M. Tamagnone, J. S. Gómez-Díaz, J. R. Mosig, and J. Perruisseau-Carrier, "Reconfigurable thz plasmonic antenna concept using a graphene stack," *Appl. Phys. Lett.*, vol. 101, 2012, Art. no. 214102.

[20] J. Yang, F. Kong, and K. Li, "Broad tunable nanoantenna based on graphene log-periodic toothed structure," *Plasmonics*, vol. 11, no. 4, pp. 981–986, Aug. 2016.

[21] K. Yao and Y. Liu, "Controlling electric and magnetic resonances for ultracompact nanoantennas with tunable directionality," *ACS Photon.*, vol. 3, no. 6, pp. 953–963, Feb. 2016.

[22] A. Radwan, V. Verri, M. D'Amico, and G. G. Gentili, "Beam reconfigurable antenna for the THz band based on a graphene high impedance surface," *Physica E, Low-Dimensional Syst. Nanostruct.*, vol. 85, pp. 316–323, 2017.

[23] X. C. Wang, W. S. Zhao, J. Hu, and W. Y. Yin, "Reconfigurable terahertz leaky wave antenna using graphene-based high-impedance surface," *IEEE Trans. Nanotechnol.*, vol. 14, no. 1, pp. 62–69, Jan. 2015.

[24] M. H. El-Sherif, M. H. Bakr, and E. A. Soliman, "E-shaped wideband plasmonic nantennas with linear and dual-linear polarizations," *Photon. Res.*, vol. 3, pp. 140–145, Aug. 2015.

[25] CST Microwave Studio. 2012. [Online]. Available: www.cst.com.

[26] D. G. Krige, "A statistical approach to some basic mine valuation problems on the witwatersrand," *J. Chem., Metallurgical, Mining Soc. South Africa*, vol. 52, no. 6, pp. 119–139, 1951.

[27] S. Koziel, J. W. Bandler, and Q. S. Cheng, "Reduced-cost microwave component modeling using space mapping-enhanced electromagnetic-based kriging surrogates," *Int. J. Numer. Model*, vol. 26, no. 3, pp. 275–286, 2013.

[28] S. N. Lophaven, H. B. Nielsen, and J. Søndergaard, "DACE - A matlab kriging toolbox," Informat. Math. Model., Technical University of Denmark, Lyngby, Denmark, Tech. Rep. IMM-REP-2002-12, 2002.

[29] V. Pareto, *Manuale Die Economia Politica*. Milano, Italy: Societa Editrice Libraria, 1906.

[30] C. C. Coello and M. Lechuga, "MOPSO: A proposal for multiple objective particle swarm optimization," in *Proc. Congr. Evol. Comput.*, 2002, pp. 1051–1056.

[31] C. A. C. Coello, G. T. Pulido, and M. S. Lechuga, "Handling multiple objectives with particle swarm optimization," *IEEE Trans. Evol. Comput.*, vol. 8, no. 3, pp. 256–279, Jun. 2004.

[32] J. P. Brans and P. Vincke, "Note—A preference ranking organisation method," *Manag. Sci.*, vol. 31, no. 6, pp. 647–656, Jun. 1985.

[33] A. S. O. Hassan and A. S. Mohamed, "Surrogate-based circuit design centering," in *Surrogate-Based Modeling and Optimization*, New York, NY, USA: Springer, 2013, pp. 27–49.

[34] H. L. Abdel-Malek, A. S. O. Hassan, E. A. Soliman, and S. A. Dakroury, "The ellipsoidal technique for design centering of microwave circuits exploiting space mapping interpolating surrogates," *IEEE Trans. Microw. Theory Techn.*, vol. 54, no. 10, pp. 3731–3738, Oct. 2006.

[35] A. S. O. Hassan, "Normed distances and their applications in optimal circuit design," *Optim. Eng.*, vol. 4, no. 3, pp. 197–213, 2003.

[36] A. S. O. Hassan, A. S. Mohamed, A. A. Rabie, and A. S. Etman, "A novel surrogate-based approach for optimal design of electromagnetic-based circuits," *Eng. Optim.*, vol. 48, no. 2, pp. 185–198, Jan. 2015.

[37] D. M. Pozar, "Power Dividers and Directional Couplers," in *Microwave Engineering*, Hoboken, NJ, USA: Wiley, 2012, pp. 362–370.

[38] C. A. Balanis, "Microstrip Antennas," in *Antenna Theory: Analysis and Design*, Hoboken, NJ, USA: Wiley, 2005, pp. 816–843.

[39] E. A. Soliman, M. H. Bakr, and N. K. Nikolova, "Accelerated gradient-based optimization of planar circuits," *IEEE Trans. Antennas Propag.*, vol. 53, no. 2, pp. 880–883, Feb. 2005.

[40] T. W. Simpson, J. D. Peplinski, P. N. Koch, and J. K. Allen, "Metamodels for computer-based engineering design: Survey and recommendations," *Eng. Comput.*, vol. 17, no. 2, pp. 129–150, Jul. 2001.

[41] K. Antreich, H. Graeb, and C. Wieser, "Circuit analysis and optimization driven by worst-case distances," *IEEE Trans. Comput.-Aided Des. Integr. Circuits Syst.*, vol. 13, no. 1, pp. 57–71, Jan. 1994.